Environmental Science and Pollution Research
https://doi.org/10.1007/s11356-024-33914-6

RESEARCH ARTICLE

Direct shear behaviors of excavated clay reinforced with geocomposite drainage layer encapsulated in thin sand layers

Lin-Jie Wang[1] · Hui Xu[1] · Jian-Wen Qian[1] · Jin-Nan Wang[1] · Liang-Tong Zhan[2]

Received: 3 January 2024 / Accepted: 2 June 2024

Abstract

The objective of this study is to assess the effectiveness of a novel structure comprising a geocomposite drainage layer and a thin sand layer (GDL + sand) in mitigating the rapid dumping of excavated clay and its associated issues, such as landslides. Two sets of direct shear tests were conducted to investigate the influence of sand layer thickness and compaction degree on the interface shear behavior of the GDL + sand structure. As the sand layer thickness increased, both the interface shear strength and friction angle gradually increased, first more sharply and then at a slower rate toward stability, while the interface cohesion decreased gradually. The optimal sand layer thickness for achieving the most effective reinforcement in stabilizing the clay was identified as 10 mm. A higher sand layer compaction degree was found to result in increased interface shear strength, interface friction angle, and interface cohesion. Building on these findings, the reinforcing efficiency of the GDL + sand structure was investigated through mechanism analysis in comparison to that of a geogrid + sand structure and GDL structure as per the interface friction coefficient. The ranking of interface friction coefficients among the three structures emerged as: geogrid + sand > GDL + sand > GDL. These results suggests that the GDL + sand structure exhibits superior reinforcement efficiency compared to the GDL structure and offers better drainage efficiency than the geogrid + sand structure.

Keywords GDL + sand structure · Excavated clay · Sand layer thickness · Sand layer compaction degree · Interface friction coefficient

Introduction

Chinese cities have extensively exploited underground spaces since the turn of the twenty-first century (Kataguiri et al. 2019). By 2017, these activities had produced a staggering two billion tons of excavated soil (Zhan et al. 2018). Currently, the primary method for disposing of excavated soil in China involves landfilling or dumping. Due to a lack of extensive construction experience and the absence of technical standards, uncontrolled dumping often leads to disasters such as landslides in soft soil regions of China (Wang et al. 2022). A tragic example unfolded in Shenzhen's Guangming New District on December 20, 2015, resulting in approximately 2.51×10^6 m^3 of excavated soil sliding out of a dump site, impacting nearly 0.38 km^2, destroying 33 buildings, and killing 77 people (Zhan et al. 2018, 2021; Yin et al. 2016). The excavated soil in such regions is characterized by high fine grain content, high water content, small permeability coefficient, and low shear strength (Tang and Liu 2014). Dangerous conditions intensify throughout the soil-filling process as dumping height increases, the soil consolidation process is sluggish and the soil shear strength increases slowly (Qian 2021). Addressing these issues requires enhancing both the drainage capacity and shear strength of fine-grained soil dumps.

Over recent decades, geosynthetic-reinforced structures have been proven successful in improving the stability of soil dumps while reducing construction costs (Yang et al. 2019; Luo et al. 2020). These structures are widely employed to strengthen embankment enhancement (Tolooiyan et al. 2009; Wang et al. 2011; Fischer 2022), retaining wall (Portelinha et al. 2013; Portelinha and Zornberg 2014; Chehade et al. 2019), and slopes (Viswanadham and König 2009; Hu

Responsible Editor: Philippe Garrigues

✉ Hui Xu
xuhui@zstu.edu.cn

[1] School of Civil Engineering and Architecture, Zhejiang Sci-Tech University, Hangzhou 310018, China

[2] MOE Key Laboratory of Soft Soils and Geoenvironmental Engineering, Zhejiang University, Hangzhou 310058, China

Published online: 04 June 2024

et al. 2010; Liu et al. 2012; Luo et al. 2018), improving overall stability through tensile reinforcement and geosynthetic/soil interactions (Liu et al. 2012; Chehade et al. 2019). The performance of reinforced soil structures hinges on the mobilization of interface shearing resistance between the soil and reinforcement. This criterion typically excludes the use of fine-grained soil as a backfill material in reinforced soil structures (Sridharan et al. 1991). However, two innovative techniques have been developed to overcome this limitation.

The first of these techniques involves the geogrid + sand structure, which incorporates reinforcement within a frictional soil layer. Various studies employing direct shear tests (Abdi et al. 2009a, 2009b), pullout tests (Sridharan et al. 1991; Abdi and Arjomand 2011; Abdi and Zandieh 2014; Abdi et al. 2021), triaxial compression tests (Unnikrishnan et al. 2002; Yang et al. 2016), centrifuge tests (Jones and Van Rooy 2014), model tests (Yang et al. 2023) and numerical modelling (Abdi and Zandieh 2014; Cui et al. 2021; Xie et al. 2022) have demonstrated that the geogrid + sand structure can effectively enhance soil-reinforcement interaction. Additionally, it establishes drainage paths that reduce pore water pressure, thereby improving the shear behavior of fine-grained soil fills. The shear strength of clay reinforced with the geogrid + sand structure increases as the number of reinforcement layers increases (Yang et al. 2016). Interestingly, the shear strength does not continually increase with increasing sand layer thickness; there is, in fact, an optimal sand layer thickness (Sridharan et al. 1991; Abdi et al. 2009a, 2009b; Abdi and Arjomand 2011; Abdi and Zandieh 2014; Xie et al. 2022). However, Jones and Van Rooy (2014) conducted centrifuge model tests to find that although geogrid reinforcement enhances load-bearing capacity by distributing the applied load to the sand layer, it deforms the broader clay layer. Further, connectivity of sand layers can be compromised by differential settlement in fine-grained soil fills, significantly reducing their drainage path functionality (Cao et al. 2021).

The second of these innovative techniques involves the geocomposite drainage layer (GDL), which consists of a drainage core wrapped in permeable geotextiles. GDL offers dual functions of reinforcement and drainage, surpassing planar geosynthetics (e.g., geogrid and geotextile) (Jang et al. 2015) in both economical and construction advantages over traditional gravel drains (Chinkulkijniwat et al. 2017). In recent years, GDL has been increasingly adopted in a wide range of geotechnical and geoenvironmental applications, including landfill cover systems (Narejo 2013; Hersey and Power 2023), paved roads (Bahador et al. 2013; Bilodeau et al. 2015; Li et al. 2017; Saride et al. 2022; Kalore and Babu 2023), reinforced soil slopes (Bhattacherjee and Viswanadham 2017, 2019; Cholewa and Plesiński 2021; Özer and Akay 2022) and walls (Bhattacherjee and Viswanadham 2019; Mamaghanian et al. 2019; Razeghi et al. 2019; Nunes et al. 2022). When GDL is utilized in soil slopes or walls, the interface shear strength properties between the GDL and soil may govern the structures' stability. However, the shear strength of GDL-clay interface may fall below that of unreinforced clay when subjected to wet and dry cycles (Chao and Fowmes 2021; Chao and Fowmes 2022). Othman et al. (2018) conducted a series of field measurements on a clayed soil-GDL interface to find that GDL application generally reduced water content and pore water pressure, though soil softening at the interface reduces shear strength due to soaking, thereby affecting the stability of the structure.

In summary, while both the geogrid + sand and GDL structures exhibit dual functions of reinforcement and drainage, they have distinct shortcomings as well. To harness their advantages and address their limitations, a novel reinforced structure, the GDL + sand structure, was developed in this study by integrating a GDL into a sand layer. Two sets of direct shear tests were conducted on excavated clayed soil (representative of typical excavated soil in soft soil regions of China) reinforced with the GDL + sand structure. Based on the test results, the effects of sand layer thickness and compaction degree on the interface shear behavior of the GDL + sand structure were analyzed. The interface friction coefficient was introduced to examine the reinforcement efficiency of the three reinforced structures: geogrid + sand, GDL, and GDL + sand.

Materials and methods

Test apparatus

The STJY-5 direct shear instrument (Hebei Luxing Anda instrument Co., LTD, China) was used in this study to measure the shear curve of the interface between sand and GDL, as illustrated in Fig. 1. The instrument consists of a shear stress system, normal stress system, and data acquisition system.

The shear stress system includes upper and lower shear boxes, an electric motor, a clamping bar, and a steel block. Both shear boxes have internal dimensions of 300 mm × 300 mm in plane and 50 mm in height. Throughout the shear process, the upper shear box was fixed in the horizontal direction while the lower shear box freely moved horizontally on the bearing rail beneath it, driven by an electric motor. The device is displacement-controlled, allowing for shear rates between 0.02 mm/min and 3 mm/min. A clamping bar anchors the geosynthetic material to the lower shear box, ensuring it remained fixed during the shearing process. Additionally, a steel block with a textured surface in the lower shear box resists the vertical displacement of the

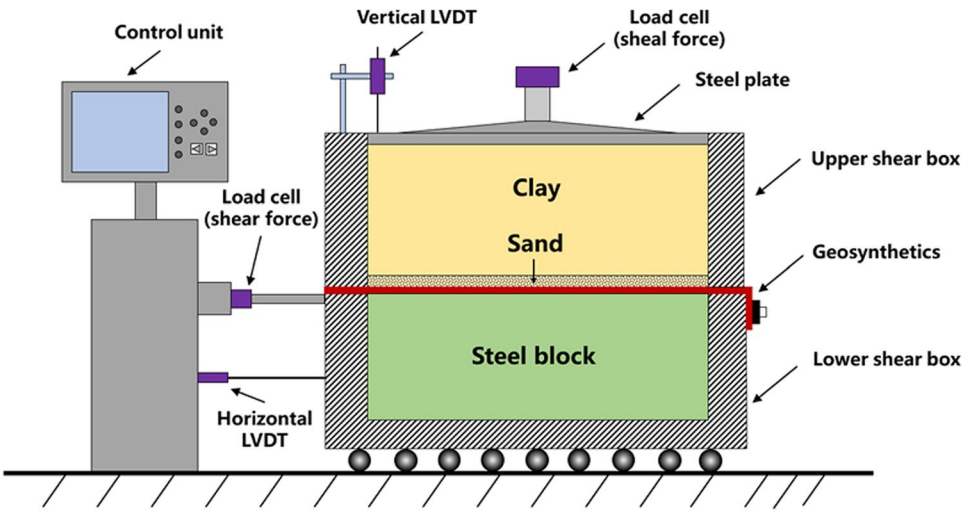

Fig. 1 Cross-section of direct shear test instrument

Table 1 Properties of clay and sand

Property	Clay	Sand
Natural moisture content (w_0, %)	35.06	12.50
Specific gravity (G_s)	2.76	2.62
Liquid limit (w_L, %)	41.81	-
Plastic limit (w_P, %)	22.72	-
Optimum moisture content (w_{opt}, %)	20.36	12.25
Maximum dry density (ρ_{dmax}, g/cm^3)	1.72	1.85

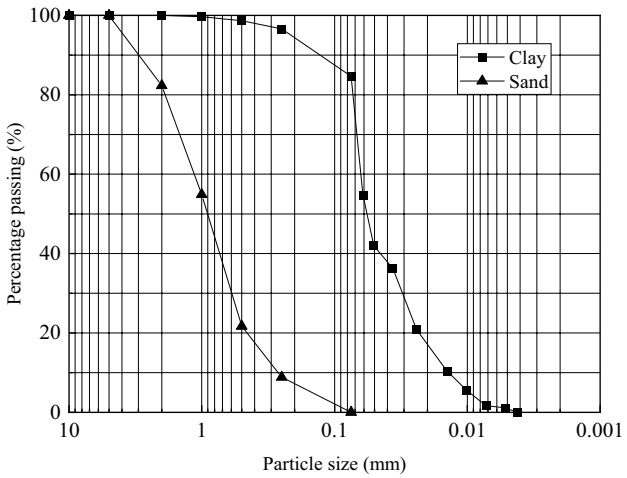

Fig. 2 Particle size distributions of clay and sand

geosynthetics and relative displacement between the geosynthetics and lower shear box. The normal stress system incorporates dead weight via a level principle for stress application and a steel plate for uniformizing the stress distribution.

The data acquisition system includes horizontal and vertical displacement transducers, as well as load cells for normal stresses and shear stresses. The horizontal displacement was recorded on a linear variable differential transformer (LVDT) with a maximum measurement of 100 mm, positioned at the front of the lower shear box. The vertical displacement was recorded using an LVDT with a maximum measurement of 50 mm, which refers to the rigid plate displacement. Normal and shear forces were measured using tension–compression sensors with load capacities of 40 kN and 10 kN, respectively. All the measurements presented in this paper were recorded digitally during the experiment.

Test materials

Two types of soils were utilized in this study: clay and sand. Their properties are summarized in Table 1 and Fig. 2. The clay was sourced from a foundation excavation engineering site in Hangzhou, representing a soil widely distributed in soft soil regions of China. The specific gravity (G_s) is 2.757, and the uniformity coefficient (C_u) and curvature coefficient (C_c) are 4.57 and 1.07, respectively. The natural moisture content (w_0) was determined to be 35.06%. The liquid limit (w_L) and plastic limit (w_P) are 41.81% and 22.72%, respectively. The consolidation coefficient ranges from 0.64×10^{-2} to 3.19×10^{-2} cm^2/s. Standard quartz sand was purchased from Fujian Province. It has a G_s of 2.624, C_u of 4.23, and C_c of 1.16. The optimum moisture content and maximum dry density were determined to be $w_{opt}=12.25\%$ and $\rho_{dmax}=1.848$ g/cm^3.

A proprietary GDL (TD60-2-E200) was utilized in this study. It is composed of a high-density polyethylene drainage core with a non-woven needle-punched polyethylene terephthalate geotextile filter thermally bonded on each side. Its main properties are summarized in Table 2.

Table 2 GDL properties

Property	GDL (TD60-2-E200)	
	Drainage core	Geotextile
Material	High-density polyethylene	Polyethylene terephthalate
Thickness (mm)	6.0	1.6
Mass per unit area (g/m^2)	940	200
Tensile strength-machine direction (kN/m)	20	10.5
Permeability (m/s)	0.87 (P)	5.4×10^{-4} (NP)

Notes: P = in plane; NP = normal to plane

Table 3 Experimental scheme

Test group	Normal stress (σ/kPa)	Thickness of sand layer (H/mm)	Compaction degree of sand layer (D_r/%)
I	25, 50, 100, 150	0, 6, 8, 10, 12, 14	85
II		10	85, 90, 95

Test procedure

Two groups of direct shear tests were conducted in this study, as outlined in Table 3. The first group was designed to examine the effects of sand layer thickness on the interface shear behavior of the GDL + sand structure. In the first group of tests, the normal stress varied from 25 to 150 kPa, the sand layer thickness varied from 0 to 14 mm, and the sand layer compaction degree was fixed at 85%. The second group was designed to investigate the effects of sand density on the interface shear behavior of the GDL + sand structure. The normal stress was kept consistent with the first group, while the sand layer compaction degree varied from 85 to 95% and the sand layer thickness was fixed at 10 mm.

Each test proceeded through the following steps:

The iron block was placed in the lower shear box, then the GDL was placed on the iron block and fixed on the sides of the lower shear box.
The sand was paved in the upper shear box to the designated thickness and compaction degree.
The clay was evenly laid over the sand layer in the upper shear box to the upper edge, then the normal stress was applied to a predetermined value.
When the clay layer reached a consolidation degree (U) of 90%, the lower shear box initiated horizontal movement at a shear rate of 1.0 mm/min until the shear displacement reached a maximum value of 30 mm.

Results and analysis

Effect of sand layer thickness on interface shear behavior of GDL + sand structure

Figure 3 presents the interface shear curves of the GDL + sand structure under different sand layer thicknesses. As the shear displacement progressed, the interface shear stress initially exhibited a rapid increase, followed by a slower increase, indicative of typical hardening behavior. Notably, the interface shear stress increased with increasing normal stress at a given sand layer thickness and a given shear displacement. For example, as the normal stress increased from 25 to 150 kPa, the interface shear stress increased from 15.11 to 64.20 kPa at sand layer thickness of 10 mm and shear displacement of 30 mm. This phenomenon can be attributed to the enhancement of interface friction resistance with increased normal stress, which restricts mutual particle adjustment and fortifies occlusal action (Ding et al. 2018).

Additionally, as sand layer thickness increased, the interface shear stress initially trended upward followed by a less noticeable change at a given normal stress and shear displacement. For instance, when the normal stress was 100 kPa and the shear displacement was 30 mm, the interface shear stress increased from 26.54 to 45.11 kPa as the sand layer thickness increased from 6 to 10 mm. However, it slightly decreased from 45.11 to 45.08 kPa as the sand layer thickness further increased from 10 to 14 mm.

Figure 4 shows the interface shear strength envelopes and parameters of the GDL + sand structure at different sand layer thicknesses. The interface shear strength was determined at a shear displacement of 30 mm. The Mohr–Coulomb strength theory was applied to calculate the interface cohesion and interface friction angle. As depicted in Fig. 4(a), the interface shear strength initially increased and then stabilized with the increase in sand layer thickness under a given normal stress. For example, at a normal stress of 150 kPa, the interface shear strength increased from 38.77 to 64.20 kPa as the sand layer thickness increased from 0 to

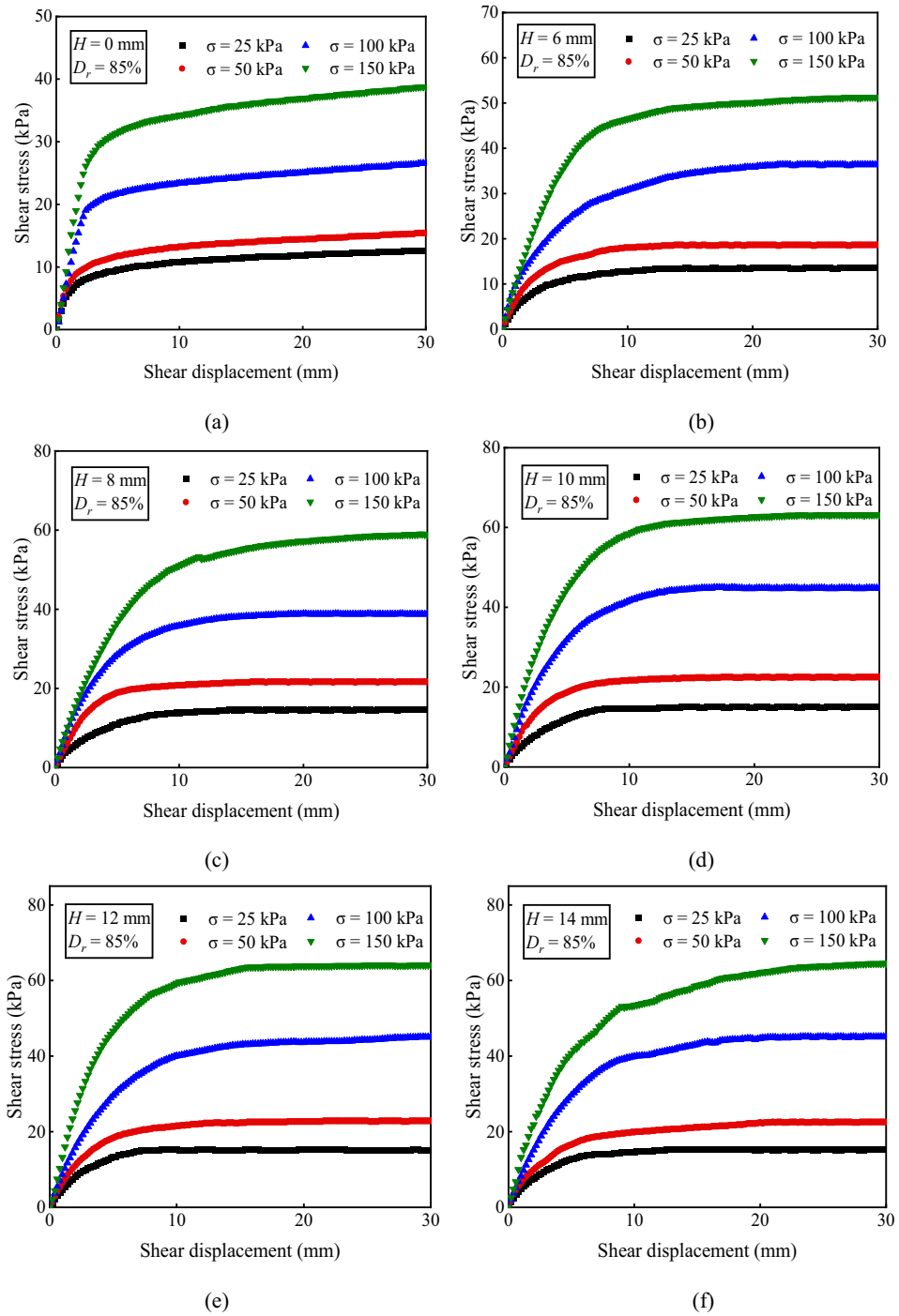

Fig. 3 Interface shear curves of GDL + sand structure under different sand layer thicknesses: (**a**) $H = 0$ mm; (**b**) $H = 6$ mm; (**c**) $H = 8$ mm; (**d**) $H = 10$ mm; (**e**) $H = 12$ mm; (**f**) $H = 14$ mm

10 mm. However, it varied around 64.20 kPa when the sand layer thickness further increased from 10 to 14 mm.

As shown in Fig. 4(b), the interface cohesion of the GDL + sand structure gradually decreased from 5.95 to 4.05 kPa as the sand layer thickness increased from 0 to 14 mm. The interface friction angle increased from 12.08° to 21.78° as the sand layer thickness increased from 0 to 10 mm, then slightly decreased to 21.99° when the sand layer thickness further increased to 14 mm. These results suggest that the provision of sand layers on both sides of the GDL effectively improves the shear strength of GDL-reinforced clay, and that 10 mm is the optimal sand layer thickness in terms of the reinforcement effect.

Once the sand layer thickness exceeds the identified optimal value of 10 mm, the interface shear strength of GDL + sand structure tends to stabilize. This finding is in line with Unnikrishnan et al. (2002) that conducted triaxial tests on geotextile + sand structure. However, Abdi et al.

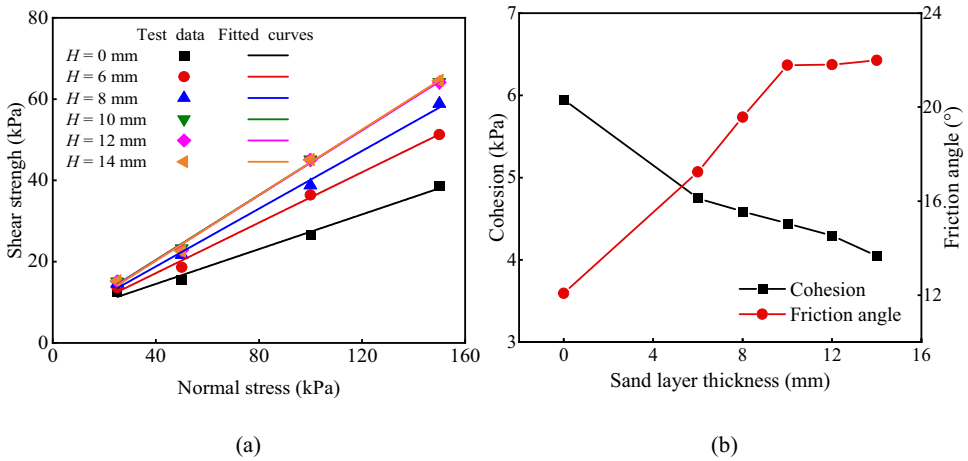

Fig. 4 Interface shear strength of GDL + sand structure at different sand layer thicknesses: (**a**) Shear strength envelopes; (**b**) Shear strength parameters

(2009b) and Liu et al. (2018) found that the interface shear strength of geogrid + sand structure tends to reduce when the sand layer thickness exceeds the identified optimal value. This phenomenon may be attributed to the presence of a shear zone within a specific range on both sides of the reinforcement during the direct shear process (Liu et al. 2018). The properties of the soil in this shear zone significantly impact the interface shear strength of the GDL + sand structure. When the sand layer is relatively thin, there are relatively few sand grains near the GDL, and some of the grains may become embedded in the clay under normal stress. Consequently, the interfacial enhancement of the GDL + sand structure is not fully realized, resulting in an increase in interface shear stress with an increase in sand layer thickness (Abdi et al. 2009a, b). When the sand layer is excessively thick, conversely, the sand-clay interface is situated far from the shear zone. Thus, the sand layer fully maximizes its role in interfacial enhancement, seemingly independent of its thickness. The different variations of the interface shear strength with the sand layer thickness exceeds the identified optimal value, may be associated with the different properties of the reinforcements used.

Effect of sand layer compaction degree on interface shear behavior of GDL + sand structure

Figure 5 shows the interface shear curves of the GDL + sand structure under different sand layer compaction degrees. The interface shear stress gradually increased with normal stress at a given sand layer compaction degree and shear displacement. For example, at a compaction degree of 85% and shear displacement of 30 mm, the interface shear stress increased from 15.11 to 64.20 kPa as the normal stress increased from 25 to 150 kPa as the normal stress increased from 25 to 150 kPa.

Furthermore, the interface shear stress increased as the sand layer compaction degree increased under a given normal stress and shear displacement. For instance, when the sand layer compaction degree increased from 85 to 95%, the interface shear stress increased from 64.20 to 85.69 kPa at normal stress of 150 kPa and shear displacement of 30 mm.

Figure 6 displays the interface shear strength envelopes and parameters of the GDL + sand structure at different sand layer compaction degrees. As shown in Fig. 6(a), the interface shear strength increased linearly with normal stress under a given compaction degree of the sand layer. Additionally, the interface shear strength increased with the sand layer compaction degree under a given normal stress. The interface cohesion and interface friction angle of the GDL + sand structure under different sand layer compaction degrees were obtained according to the Mohr–Coulomb criterion, as shown in Fig. 6(b). As the sand layer compaction degree increased, the interface friction angle increased gradually while the interface cohesion did not markedly change. When the sand layer compaction degree increased from 85 to 95%, the interface friction angle increased from 21.78° to 28.12° while the interface cohesion slightly increased from 4.44 to 5.06 kPa.

The inter-particle pores were reduced by an increase in the sand layer compaction degree, resulting in a more compact arrangement of sand particles and an augmented effective contact area. This phenomenon restricted the mutual adjustment of sand particles and enhanced the occlusion. At this point, the friction resistance faced by the sand particles in proximity to the GDL increased, leading to an increase in the interface friction angle (Ma et al. 2020; Ding et al. 2018; Liu et al. 2018). Interface cohesion, which is considered independent of normal stress, mainly arises from the lateral confining effect of reinforcement materials on soil (Li et al. 2018). It is influenced by the type of reinforcement material, the particle size distribution of the soil, and the contact points between the reinforcement and soil (Fakhrabadi et al. 2021; Xu et al.

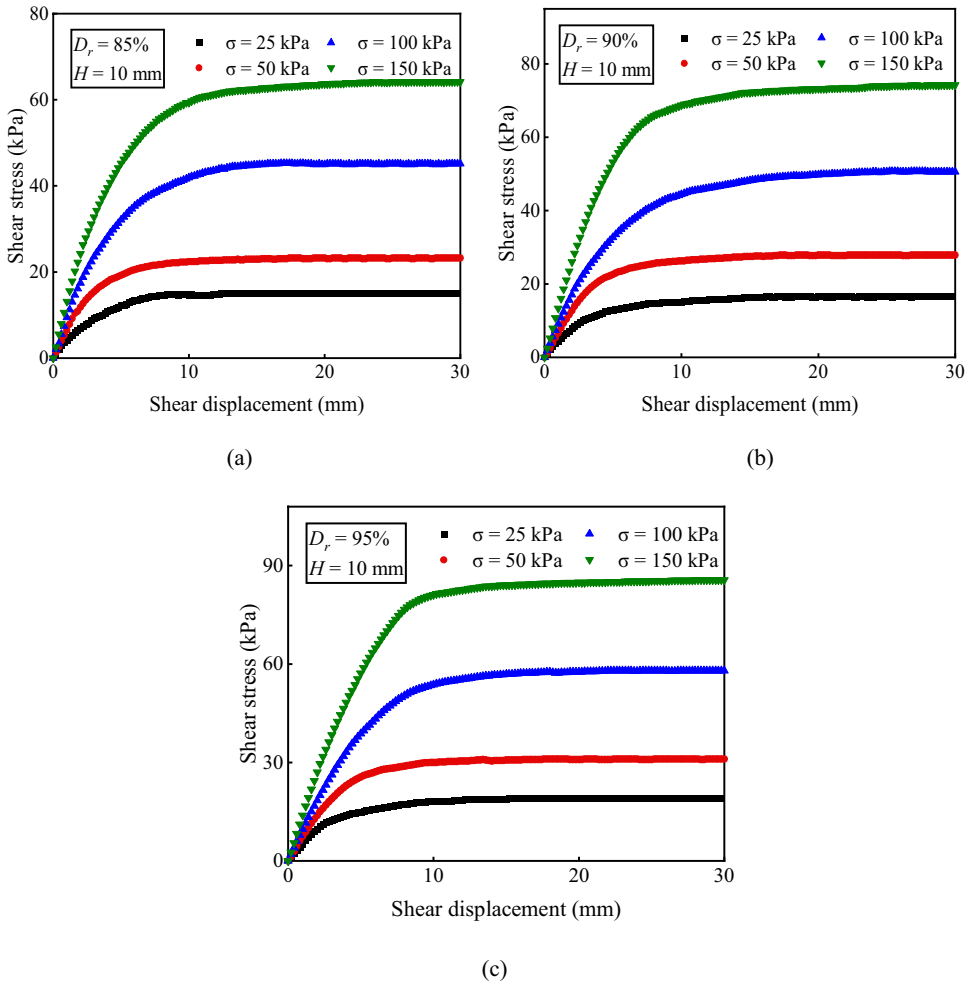

Fig. 5 Interface shear curves of GDL + sand structure under different sand layer compaction degrees: (**a**) D_r = 85%; (**b**) D_r = 90%; (**c**) D_r = 95%

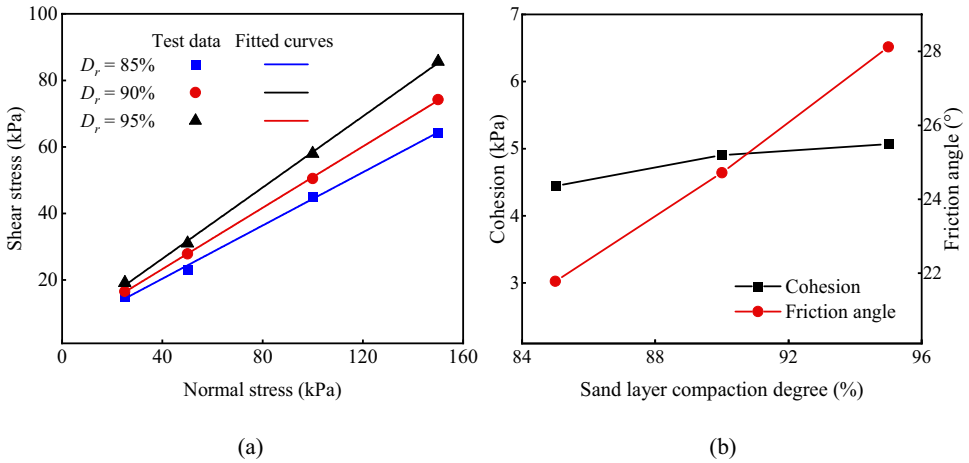

Fig. 6 Interface shear strength at different sand layer compaction degrees: (**a**) Shear strength envelopes; (**b**) Shear strength parameters

2023; Hassan et al. 2023). A higher sand layer compaction degree results in more intense interface interactions and,

therefore, higher interface cohesion (Anda et al. 2023).

Comparisons of different reinforced structures in improving shear strength of clay layer

Interface friction coefficient of GDL + sand layer

The interface friction coefficient, defined as the ratio of the peak shear stress to the normal stress of the reinforcement-soil composite, is a comprehensive strength parameter reflecting the friction effect between the reinforcement and soil (Gao et al. 2021; Xu et al. 2022; Chen et al. 2022; Bai et al. 2022). Unlike the traditional friction coefficient expressed solely by an internal friction angle (Gao et al. 2021), the interface friction coefficient serves as an index to evaluate the friction characteristics of different reinforced soil interfaces. It can be calculated as follows:

$$f^* = \frac{\tau_{sg}}{\sigma_n} \tag{1}$$

where f^* is the interface friction coefficient, σ_n is the normal stress, and τ_{sg} is the interface shear stress corresponding to σ_n.

Figure 7 depicts the influence of the thickness and compaction degree of sand layer on the interface friction coefficient of the GDL + sand structure. As shown in Fig. 7(a), the interface friction coefficient increased with sand layer thickness at a given normal stress, with the upward trend transitioning from steep to more gradual. For example, f^* increased from 0.26 to 0.43 as the sand layer thickness increased from 0 to 10 mm, then remained nearly unchanged as the sand layer thickness further increased to 14 mm.

This observation aligns with the variations in interface shear strength with sand layer thickness. It is primarily attributed to the fact that the optimal sand layer thickness is achieved at 10 mm. The sand layer is most effective in terms of reinforcement at this point; beyond 10 mm, increases in sand layer thickness do not effectively enhance the interface shear strength. Figure 7(b) shows that the interface friction coefficient increased linearly as the sand layer compaction degree increased at a given normal stress. The linear-regression analysis results indicate a close increase rate for various cases at different normal stresses, ranging from 0.013 to 0.016.

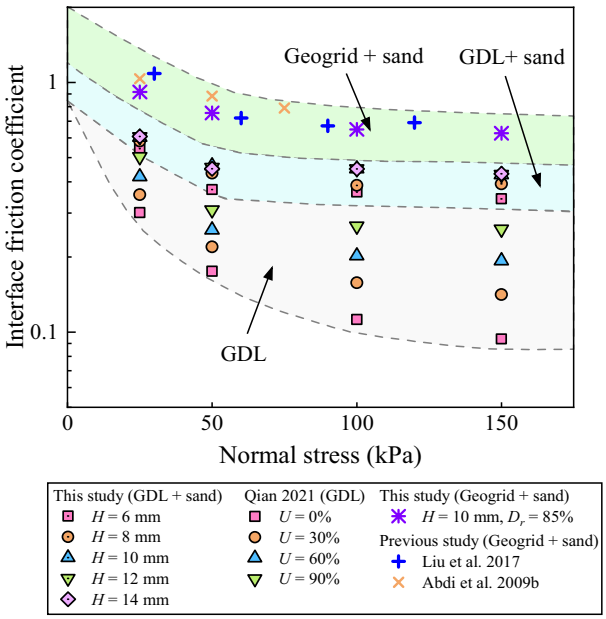

Fig. 8 Interface friction coefficient of GDL and GDL + sand structures

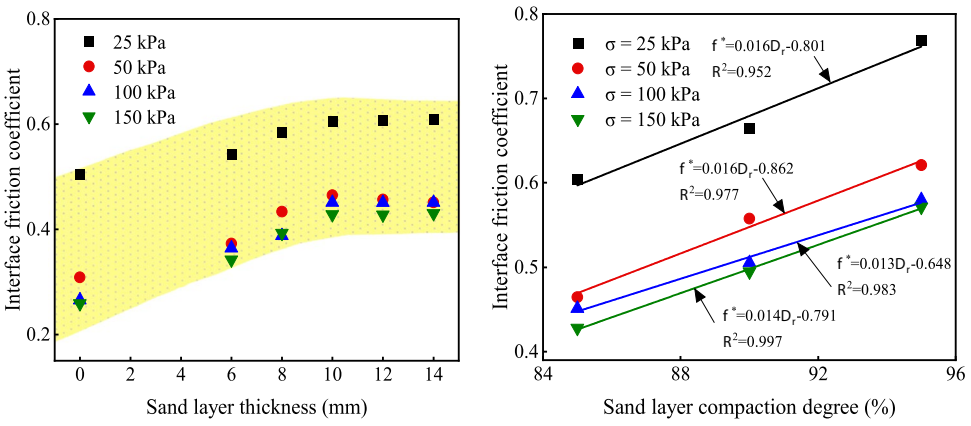

(a) (b)

Fig. 7 Variations in interface friction coefficient with different factors: (**a**) Sand layer thickness at $D_r = 85\%$; (**b**) Sand layer compaction degree at $H = 10$ mm

Comparison of interface friction coefficient for different reinforced structures

Figure 8 presents a comparison of interface friction coefficients among three structures: geogrid + sand, GDL + sand, and GDL. Direct shear tests on the geogrid + sand structure and GDL structure were also conducted. The same sand and clay were used in these tests as in the GDL + sand structure, with a polypropylene biaxially oriented geogrid (model TGSG15-15) adopted in the geogrid + sand structure. The tests were conducted at different clay layer consolidation degrees for the GDL structure, with a sand layer thickness of 10 mm, sand layer compaction degree of 85%, and clay layer consolidation degree of 90% for the geogrid + sand structure.

Overall, the interface friction coefficient decreased with increasing normal stress, and the downward trend transitioned from steep to gradual. Equation (1) can be rewritten accordingly as $f^* = \tan\varphi + c/\sigma$, where φ and c refer to the interface friction angle and interface cohesion, respectively. Evidently, f^* tends toward the value of $\tan\varphi$, i.e., $f^*_{\mathrm{lim}} = \tan\varphi$.

For clay reinforced with GDL, the decreasing rate of interface friction coefficient tended to be smaller and the value of f^*_{lim} tended to be larger as the clay layer consolidation degree increased. This is mainly because an increase in the interface friction angle and decrease in the interface cohesion decreases occurred as the consolidation degree of the clay layer increased (Qian 2021).

Figure 8 illustrates where the interface friction coefficient of the GDL structure is smaller than that of the GDL + sand structure regardless of the clay layer consolidation degree (U) under a given normal stress. This suggests that introducing a sand layer between the clay and GDL effectively enhances the interface shear strength. In this text, a portion of the sand (replacing the clay) became embedded in the grooves of the GDL, establishing a robust bonding relationship at the GDL-sand interface. Additionally, Fig. 8 shows where the interface friction coefficient of the geogrid + sand structure generally exceeded that of the GDL + sand structure.

Liu et al. (2017) and Abdi et al. (2009b) conducted interface shear tests on a geogrid + sand structure, which exhibited similar interface friction coefficients as in the present study, although the properties of the sand used in these experiments differ. This can be attributed to the fact that grid-type reinforcements are more effective than sheet-type reinforcements due to the interlocking effect of sand within grid openings (Unnikrishnan et al. 2002).

In summary, the interface friction coefficients for the three reinforced structures at a consistent normal stress can be ranked as geogrid + sand > GDL + sand > GDL. When only considering the reinforcement effect, the geogrid + sand structure is the optimal choice for fine-grained soil dump applications. However, the fine-grained soil particles would either fill into the spaces between sand particles or flow away with drainage under water infiltration conditions. As a result, the drainage function of the geogrid + sand structure may weaken significantly due to clogging (Cao et al. 2021). Fine-grained soils are also susceptible to tension cracks, and the differential deformation of these soils may cause disconnection of the sand layer, hindering effective drainage in the geogrid + sand structure. GDL consists of a drainage core with two nonwoven geotextiles firmly bonded on the top and bottom. This drainage core creates a seepage path, which is kept unclogged by the nonwoven geotextiles (Kalore and Babu 2023). Therefore, the GDL structure can mitigate the aforementioned issues through its geogrid + sand structure. Furthermore, a thin sand layer on both sides of GDL appears to be effective in improving the shear strength of reinforced clay (Yang et al. 2016). Therefore, the GDL + sand structure is an effective, practical solution in fine-grained soil dumps.

Conclusions

In this study, the effects of sand layer thickness and compaction degree on the interface shear behavior of a GDL + sand structure were investigated through two sets of direct shear tests. The effectiveness and efficiency of three reinforced structures (geogrid + sand, GDL + sand, and GDL) were examined according to the interface friction coefficient index. The key findings of this work can be summarized as follows:

(1) The interface shear curve of the GDL + sand structure exhibited typical hardening behavior. The interface shear stress increased with increasing normal stress at a given shear displacement and sand layer thickness/compaction degree. This behavior can be attributed to increased interface friction resistance at larger normal stress, limited mutual particle adjustment, and strengthened occlusal action.

(2) Increasing the sand layer thickness from 0 to 10 mm caused an increase in the interface shear strength of the GDL + sand structure at a given normal stress. This is mainly due to the interface friction angle, which increased from 12.08 to 21.78; the decrease in interface cohesion from 5.95 to 4.44 kPa had a less pronounced effect. As the sand layer thickness further increased to 14 mm, the interface shear strength stabilized alongside a further slight increase in the interface friction angle to 21.99° and continuous decline in interface cohesion to 4.05 kPa. The optimal sand layer thickness for achieving the optimal reinforcement of clay in this study was identified at 10 mm for the GDL + sand structure.

(3) The interface shear strength of the GDL + sand structure increased as the sand layer compaction degree increased under a given normal stress. When the compaction degree increased from 85 to 95%, the interface friction angle increased from 21.78° to 28.12°, while the interface cohesion increased from 4.44 to 5.06 kPa. This is mainly related to the increased interface friction resistance caused by the more compact arrangement of sand particles and an augmented effective contact area.

(4) The interface friction coefficient increased, first sharply and then slowly, with increasing sand layer thickness under a given normal stress. This is consistent with the changes in interface shear strength. However, it increased approximately linearly with the sand layer compaction degree between 0.013 and 0.016. The interface friction coefficient decreased, steeply then slowly, with normal stress and tended toward the value of $\tan\varphi$.

(5) The interface friction coefficients for the three reinforced structures at a given normal stress fall into order as: geogrid + sand > GDL + sand > GDL. When applied in fine-grained soil dumps, the geogrid + sand structure is prone to clogging or fracture under water infiltration conditions due to the migration of fine particles, significantly reducing the drainage efficiency. In contrast, GDL can provide complete seepage paths via its drainage core and protect the seepage path against clogging via nonwoven geotextiles. Consequently, the GDL + sand structure is recommended as an optimal practical solution to improve the drainage capacity and shear strength of fine-grained soil dumps.

This study has limitations that may be addressed in future research efforts. Firstly, the findings obtained here are based on the behavior of excavated clay combined with a sand layer of optimal thickness. It is important to note that variations in soil type and the characteristics of the sand and GDL could lead to different shear behaviors at the GDL-sand interface, thus altering the optimal thickness of the sand layer. Secondly, environmental factors like rainfall infiltration, seismic activity, drying-wetting cycles, and freeze–thaw cycles are likely to significantly impact the interface shear behavior of the GDL + sand structure. The research team plans to investigate these factors in upcoming studies.

Author contributions Lin-Jie Wang: Investigation, Validation, Data curation, Writing-original draft. Hui Xu: Conceptualization, Methodology, Funding acquisition, Supervision. Jian-Wen Qian: Investigation, Data curation, Visualization. Jin-Nan Wang: Writing—review & editing, Data curation. Liang-Tong Zhan: Writing—review & editing, Supervision.

Funding The authors are very grateful for the financial support of the National Natural Science Foundation of China (Grant No. 42172309).

Data Availability The original contributions presented in the study are included in the article, further inquiries can be directed to the corresponding author.

Declarations

Ethics approval The authors confirmed that this manuscript has not been published somewhere else and is not under consideration by another journal. Thus, informed consent and ethical approval do not apply for this research.

Consent to participate Not applicable.

Consent for publication Not applicable.

Competing interests The authors declare no competing interests.

References

Abdi MR, Arjomand MA (2011) Pullout tests conducted on clay reinforced with geogrid encapsulated in thin layers of sand. Geotext Geomembr 29(6):588–595. https://doi.org/10.1016/j.geotexmem.2011.04.004

Abdi MR, Sadrnejad SA, Arjomand MA (2009a) Clay reinforcement using geogrid embedded in thin layers of sand. Intl J Civil Eng 7(4): 224–235. https://sid.ir/paper/271819/en

Abdi MR, Sadrnejad A, Arjomand MA (2009b) Strength enhancement of clay by encapsulating geogrids in thin layers of sand. Geotext Geomembr 27(6):447–455. https://doi.org/10.1016/j.geotexmem.2009.06.001

Abdi MR, Zandieh AR (2014) Experimental and numerical analysis of large scale pull out tests conducted on clays reinforced with geogrids encapsulated with coarse material. Geotext Geomembr 42(5):494–504. https://doi.org/10.1016/j.geotexmem.2014.07.008

Abdi MR, Zandieh AR, Mirzaeifar H, Arjomand MA (2021) Influence of geogrid type and coarse grain size on pull out behaviour of clays reinforced with geogrids embedded in thin granular layers. Eur J Environ Civ Eng 25(12):2161–2180. https://doi.org/10.1080/19648189.2019.1619627

Anda R, Wang L, Ying MJ, Huang YT (2023) Analysis of Shear Characteristics of Recycled Concrete Aggregate-Geogrid Interface. J Mater Civ Eng 35(7):04023169. https://doi.org/10.1061/JMCEE7.MTENG-15365

Bahador M, Evans TM, Gabr MA (2013) Modeling effect of geocomposite drainage layers on moisture distribution and plastic deformation of road sections. J Geotech Geoenviron Eng 139(9):1407–1418. https://doi.org/10.1061/(ASCE)GT.1943-5606.0000877

Bai Q, Liu J, Wang Y, Du H, Wang B (2022) Experimental Investigation of Interface Characteristics between Geogrid and Coarse-Grained Soil in a Seasonally Frozen Area. Appl Sci 12(19):10187. https://doi.org/10.3390/app121910187

Bhattacherjee D, Viswanadham BVS (2017) Effect of Geocomposite Layers on Slope Stability Under Rainfall Condition. Indian Geotech J 2(48):316–326. https://doi.org/10.1007/s40098-017-0280-4

Bhattacherjee D, Viswanadham BVS (2019) Centrifuge model studies on performance of hybrid geosynthetic–reinforced slopes with poorly draining soil subjected to rainfall. J Geotech Geoenviron Eng 145(12):04019108. https://doi.org/10.1061/(ASCE)GT.1943-5606.0002168

Bilodeau JP, Doré G, Savoie C (2015) Laboratory evaluation of flexible pavement structures containing geocomposite drainage layers

using light weight deflectometer. Geotext Geomembr 43(2):162–170. https://doi.org/10.1016/j.geotexmem.2015.02.002
Cao DF, Zhu HH, Guo CC, Wu JH, Fatahi B (2021) Investigating the hydro-mechanical properties of calcareous sand foundations using distributed fiber optic sensing. Eng Geol 295:106440. https://doi.org/10.1016/j.enggeo.2021.106440
Chao Z, Fowmes G (2021) Modified stress and temperature-controlled direct shear apparatus on soil-geosynthetics interfaces. Geotext Geomembr 49(3):825–841. https://doi.org/10.1016/j.geotexmem.2020.12.011
Chao Z, Fowmes G (2022) The short-term and creep mechanical behaviour of clayey soil-geocomposite drainage layer interfaces subjected to environmental loadings. Geotext Geomembr 50(2):238–248. https://doi.org/10.1016/j.geotexmem.2021.10.004
Chehade HA, Dias D, Sadek M, Jenck O, Chehade FH (2019) Seismic analysis of geosynthetic-reinforced retaining wall in cohesive soils. Geotext Geomembr 47(3):315–326. https://doi.org/10.1016/j.geotexmem.2019.02.003
Chen C, Yang Q, Leng W, Dong J, Xu F, Wei L, Ruan B (2022) Experimental investigation of the mechanical properties of the sand–concrete pile interface considering roughness and relative density. Materials 15(13):4480. https://doi.org/10.3390/ma15134480
Chinkulkijniwat A, Horpibulsuk S, Van Bui D, Udomchai A, Goodary R, Arulrajah A (2017) Influential factors affecting drainage design considerations for mechanical stabilised earth walls using geocomposites. Geosynth Int 24(3):224–241. https://doi.org/10.1680/jgein.16.00027
Cholewa M, Plesiński K (2021) Performance Comparison of Geodrain Drainage and Gravel Drainage Layers Embedded in a Horizontal Plane. Materials 14(21):6321. https://doi.org/10.3390/ma14216321
Cui L, Cao W, Sheng Q, Xie M, Yang T, Xiao P (2021) Analysis of Layered Geogrids–Sand–Clay Reinforced Structures under Triaxial Compression by Discrete Element Method. Appl Sci 11(21):9952. https://doi.org/10.3390/app11219952
Ding LQ, Li DY, Chen FQ (2018) Experimental study on the properties of interface between geogrid and saturated fine sand. J Yangtze River Sci Res Instit 35(11): 101. https://doi.org/10.11988/ckyyb.20170474
Fakhrabadi A, Ghadakpour M, Choobbasti AJ, Kutanaei SS (2021) Influence of the non-woven geotextile (NWG) on the engineering properties of clayey-sand treated with copper slag-based geopolymer. Constr Build Mater 306:124830. https://doi.org/10.1016/j.conbuildmat.2021.124830
Fischer S (2022) Geogrid reinforcement of ballasted railway superstructure for stabilization of the railway track geometry–A case study. Geotext Geomembr 50(5):1036–1051. https://doi.org/10.1016/j.geotexmem.2022.05.005
Gao Y, Hang L, He J, Zhang F, Van Paassen L (2021) Pullout behavior of geosynthetic reinforcement in biocemented soils. Geotext Geomembr 49(3):646–656. https://doi.org/10.1016/j.geotexmem.2020.10.028
Jana K, Hazari S, Ghosh S (2021) Experimental and numerical studies of three-layered unreinforced and geosynthetic-reinforced soil slopes. Innov Infrastr Solut 6(1):41. https://doi.org/10.1007/s41062-020-00408-6
Jang YS, Kim B, Lee JW (2015) Evaluation of discharge capacity of geosynthetic drains for potential use in tunnels. Geotext Geomembr 43(3):228–239. https://doi.org/10.1016/j.geotexmem.2015.03.001
Jones BR, Van Rooy JL (2014) Behaviour of a thin compressible clay horizon under geogrid reinforced sand with a wide platform load. Engineering Geology for Society and Territory–Volume 4: Marine and Coastal Processes, Springer, Cham, pp.51–54. https://doi.org/10.1007/978-3-319-08660-6_10
Kalore SA, Babu GS (2023) Hydraulic design of granular and geocomposite drainage layers in pavements based on demand-capacity modeling. Geotext Geomembr 51(5):131–143. https://doi.org/10.1016/j.geotexmem.2023.06.001
Kataguiri K, Boscov MEG, Teixeira CE, Angulo SC (2019) Characterization flowchart for assessing the potential reuse of excavation soils in Sao Paulo city. J Clean Prod 240:118215. https://doi.org/10.1016/j.jclepro.2019.118215
Hassan W, Farooq K, Mujtaba H, Alshameri B, Shahzad A, Nawaz MN, Azab M (2023) Experimental investigation of mechanical behavior of geosynthetics in different soil plasticity indexes. Transport Geotech 39:100935. https://doi.org/10.1016/j.trgeo.2023.100935
Hersey D, Power C (2023) Assessing the importance of drainage layers over geomembrane liners within engineered cover systems: Seven years of field monitoring at three mine waste rock piles. Geotext Geomembr 51(3):381–389. https://doi.org/10.1016/j.trgeo.2023.100935
Hu Y, Zhang G, Zhang JM, Lee CF (2010) Centrifuge modeling of geotextile-reinforced cohesive slopes. Geotext Geomembr 28(1):12–22. https://doi.org/10.1016/j.geotexmem.2009.09.001
Li C, Ashlock J, White D, Vennapusa P (2017) Permeability and stiffness assessment of paved and unpaved roads with geocomposite drainage layers. Appl Sci 7(7):718. https://doi.org/10.3390/app7070718
Li L, Cui F, Xiao H, Ma Q, Qin L (2018) Shear performance of waste tires, geogrid and geocell reinforced soils. In Proceedings of GeoShanghai 2018 International Conference: Ground Improvement and Geosynthetics. Springer Singapore pp. 463–472. https://doi.org/10.1007/978-981-13-0122-3_51
Liu CN, Yang KH, Ho YH, Chang CM (2012) Lessons learned from three failures on a high steep geogrid-reinforced slope. Geotext Geomembr 34:131–143. https://doi.org/10.1016/j.geotexmem.2012.05.003
Liu, F.Y., Zhang, R.Y. Wang, J. (2018) Cyclic and post-cyclic direct shear behavior of sandwich reinforcement-soil interface under different sand particle sizes. Journal of Shanghai University/Shanghai Daxue Xuebao 24(3):456–466. https://doi.org/10.19721/j.cnki.1001-7372.2017.05.005
Liu FY, Zhang T, Shi J (2017) Cyclic shear behavior on soil-geogrid Interface of sandwich reinforced soil. China J Highway Transp 30(5):38–43. https://doi.org/10.19721/j.cnki.1001-7372.2017.05.005
Luo F, Zhang G, Liu Y, Ma C (2018) Centrifuge modeling of the geotextile reinforced slope subject to drawdown. Geotext Geomembr 46(1):11–21. https://doi.org/10.1016/j.geotexmem.2017.09.001
Luo F, Huang R, Zhang G (2020) Centrifuge modeling of the geogrid-reinforced slope subjected to differential settlement. Acta Geotechnica 15:3027–3040. https://doi.org/10.1007/s11440-020-01010-x
Ma LJ, Wang HY, Chai PX, Sun XR, Mai WH (2020) Experimental study on frictional characteristics of interface between geobag material and agro-ditch slope soil. Water Resour Hydropower Eng 51(9):173–180. https://doi.org/10.13928/j.cnki.wrahe.2020.09.020
Mamaghanian J, Viswanadham BVS, Razeghi HR (2019) Centrifuge model studies on geocomposite reinforced soil walls subjected to seepage. Geosynth Int 26(4):371–387. https://doi.org/10.1680/jgein.19.00018
Narejo D (2013) Finite element analysis experiments on landfill cover drainage with geosynthetic drainage layer. Geotext Geomembr 38:68–72. https://doi.org/10.1016/j.geotexmem.2013.04.001
Nunes GB, Portelinha FHM, Futai MM, Yoo C (2022) Numerical study of the impact of climate conditions on stability of geocomposite and geogrid reinforced soil walls. Geotext Geomembr 50(4):807–824. https://doi.org/10.1016/j.geotexmem.2022.04.004

Othman M, Frost M, Dixon N (2018) Stability performance and interface shear strength of geocomposite drain/soil systems. AIP Conference Proceedings, pp.23–24. https://doi.org/10.1063/1.5022943

Özer AT, Akay O (2022) Investigation of drainage function of geosynthetics for basal-reinforced embankments. Intl J Phys Modell Geotech 22(5):260–278. https://doi.org/10.1680/jphmg.21.00032

Portelinha FHM, Bueno BDS, Zornberg JG (2013) Performance of nonwoven geotextile-reinforced walls under wetting conditions: laboratory and field investigations. Geosynth Int 20(2):90–104. https://doi.org/10.1680/gein.13.00004

Portelinha FHM, Zornberg JG (2014) Development of capillary barriers during water infiltration in a geotextile-reinforced soil wall. In Proceedings of 10th International Conference of Geosynthetics. pp 1–7. https://api.semanticscholar.org/CorpusID:132441212

Qian JW (2021) Characteristics of interface between excavated soils and drainage reinforcement and optimal design of reinforced slope in soft soil area. Master degree thesis, Zhejiang Sci-Tech University, Hangzhou. https://doi.org/10.27786/d.cnki.gzjlg.2021.000328

Razeghi HR, Viswanadham BVS, Mamaghanian J (2019) Centrifuge and numerical model studies on the behaviour of geogrid reinforced soil walls with marginal backfills with and without geocomposite layers. Geotext Geomembr 47(5):671–684. https://doi.org/10.1016/j.geotexmem.2019.103470

Saride S, Huchegowda BK, Vyas S (2022) Evaluation of drainage coefficients for 2D and 3D− geocomposite embedded subbase layers. Geotext Geomembr 50(6):1110–1119. https://doi.org/10.1016/j.geotexmem.2022.07.003

Sridharan A, Murthy BS, Bindumadhava, Revanasiddappa K (1991) Technique for using fine-grained soil in reinforced earth. J Geotech Eng 117(8):1174–1190. https://doi.org/10.1061/(ASCE)0733-9410(1991)117:8(1174)

Tang Y, Liu J (2014) Engineering-Geology Zoning and Risk Assessment of Hazards in Tianjin Central Fishing Port. Engineering Geology for Society and Territory- Volume 4: Marine and Coastal Processes, pp.125–129. https://doi.org/10.1007/978-3-319-08660-6_24

Tolooiyan A, Abustan I, Selamat MR, Ghaffari S (2009) A comprehensive method for analyzing the effect of geotextile layers on embankment stability. Geotext Geomembr 27(5):399–405. https://doi.org/10.1007/978-3-319-08660-6_24

Unnikrishnan N, Rajagopal K, Krishnaswamy NR (2002) Behaviour of reinforced clay under monotonic and cyclic loading. Geotext Geomembr 20(2):117–133. https://doi.org/10.1016/S0266-1144(02)00003-1

Viswanadham BVS, König D (2009) Centrifuge modeling of geotextile-reinforced slopes subjected to differential settlements. Geotext Geomembr 27(2):77–88. https://doi.org/10.1016/j.geotexmem.2008.09.008

Wang JN, Xu H, Zhan LT, Li SZ, Wang LN (2022) Stability Satisfied Design and Construction of Excavated Soil Dumps in a Soft Soil Region in China. Front Earth Sci 9:822511. https://doi.org/10.3389/feart.2021.822511

Wang L, Zhang G, Zhang JM (2011) Centrifuge model tests of geotextile-reinforced soil embankments during an earthquake. Geotext Geomembr 29(3):222–232. https://doi.org/10.1016/j.geotexmem.2010.11.002

Xie M, Zheng J, Cao W, Dong X, Yang T, Cui L (2022) Mesoscopic pullout behavior of geosynthetics–sand–clay layered reinforced structures using discrete element method. Acta Geotech 17(6):2533–2552. https://doi.org/10.1007/s11440-021-01422-3

Xu L, Wang R, Liu Q, Chen J, Wang X, Meng Q (2023) Effect of particle size distribution on monotonic direct shear characteristics of geotextile/geogrid-calcareous sand interface. Appl Ocean Res 137:103601. https://doi.org/10.1016/j.apor.2023.103601

Xu L, Wang R, Xu D, Wang J, Wang X, Meng Q (2022) Interface Shear Behavior of Geogrid-Reinforced Calcareous Sand Under Large-Scale Monotonic Direct Shear. Intl J Geosynth Ground Eng 8(5):66. https://doi.org/10.1007/s40891-022-00403-0

Yang KH, Thuo JN, Chen JW, Liu CN (2019) Failure investigation of a geosynthetic-reinforced soil slope subjected to rainfall. Geosynth Int 26(1):42–65. https://doi.org/10.1680/jgein.18.00035

Yang KH, Wu HM, Tseng TL, Yoo C (2023) Model tests of geosynthetic-reinforced soil walls with marginal backfill subjected to rainfall. Geotext Geomembr 51(2):342–359. https://doi.org/10.1016/j.geotexmem.2022.12.002

Yang KH, Yalew WM, Nguyen MD (2016) Behavior of geotextile-reinforced clay with a coarse material sandwich technique under unconsolidated-undrained triaxial compression. Int J Geomech 16(3):04015083. https://doi.org/10.1061/(ASCE)GM.1943-5622.0000611

Yin Y, Li B, Wang W, Zhan L, Xue Q, Gao Y, Zhang N, Chen HQ, Liu TK, Li A (2016) Mechanism of the December 2015 catastrophic landslide at the Shenzhen landfill and controlling geotechnical risks of urbanization. Engineering 2(2):230–249. https://doi.org/10.1016/J.ENG.2016.02.005

Zhan LT, Zhang Z, Chen YM, Chen R, Zhang S, Liu J, Li AG (2018) The 2015 Shenzhen catastrophic landslide in a construction waste dump: Reconstitution of dump structure and failure mechanisms via geotechnical investigations. Eng Geol 238:15–26. https://doi.org/10.1016/j.enggeo.2018.02.019

Zhan LT, Guo XG, Sun QQ, Chen YM, Chen ZY (2021) The 2015 Shenzhen catastrophic landslide in a construction waste dump: analyses of undrained strength and slope stability. Acta Geotech 16(4):1247–1263. https://doi.org/10.1007/s11440-020-01083-8